Supporting Information

Intrinsic Halide Segregation at Nanometer Scale Determines the High-Efficiency of mixed cation/mixed halide Perovskite Solar Cells.

Paul Gratia[1], Giulia Grancini[1] *, Jean-Nicolas Audinot[2], Xavier Jeanbourquin[3], Edoardo Mosconi[4], Iwan Zimmermann[1], David Dowsett[2], Yonghui Lee[1], Michael Grätzel[5], Filippo de Angelis[4], Kevin Sivula[3], Tom Wirtz[2] and Mohammad Khaja Nazeeruddin[1] *

1. Experimental Methods

Sample preparation: *Mixed perovskite:* Conductive FTO glass (NSG10) was sequentially cleaned by sonication in a 2 % Hellmanex solution and isopropanol for 15 min respectively. A 30 nm titania blocking layer was applied on the substrates by spraying a solution of titanium diisopropoxide bis(acetylacetonate) in ethanol at 450 °C. In order to obtain a ~200 nm mesoporous TiO_2 layer, 30 NR-D titania paste from Dyesol diluted in ethanol (ratio 1:8 by weight) was spin-coated at 2000 rpm for 10s followed by a sintering step at 500 °C for 20 min. Subsequently, the substrates were Lithium-treated by spin-coating 60 µl of a solution of Tris(bis(trifluoromethylsulfonyl)imide) (Li-TFS) in acetonitrile (10mg/ml) onto the mesoporous layer, followed by a sintering step at 500 °C for 10 min to decompose the Li-salt as previously described[1]. The perovskite layers were fabricated using a single step spin-coating procedure reported by Seok et al[2]. For the perovskite precursor solution 508 mg of PbI_2(TCI), 68 mg PbI_2 (TCI), 180.5 mg formamidinium iodide (Dyesol) and 20.7 mg methylammonium bromide (Dyesol) were dissolved in a 1:4 mixture of DMSO:DMF. The perovskite solution was spun at 5000 rpm for 30s using a ramp of 3000rpms-1. 15s prior to the end of the spin-coating sequence, 100 µl chlorobenzene were poured onto the spinning substrate. Afterwards the substrates were transferred onto a heating plate and annealed at 100 °C for 50 min. Full devices were fabricated using the hole- transporting material polytriarylamine (PTAA). The solution was prepared in toluene (10mg/ml) using

the additive Li-bis(trifluoromethanesulfonyl) imide (from a 170 mg/ml Li-TFSI/acetonitrile stock solution) and 4 µl of 4-tert-butylpyridine (TBP). The final HTM solutions were spin-coated on top of the perovskite layers at 3000 rpm for 30 s. The gold electrodes were deposited by thermal evaporation (Kurt Lesker) of 100 nm gold using a shadow mask under high vacuum conditions.

$FAPbI_3$ perovskite: anode preparation same as for mixed perovskite devices. Precursor solution prepared following recipe described elsewhere[3]. *$MAPbI_3$ perovskite*: Anode preparation same as for mixed perovskite devices. The perovskite precursor solution contained PbI_2 (TCI, 507mg) and Methylammonium Iodide (synthesized in-house, 159mg) in 800 microliter DMSO (Acros). The Spin coating procedure was the same as for the mixed perovskite.

HIM-SIMS: We use the HIM-SIMS that was recently developed at the Luxembourg Institute of Science and Technology as a unique technique for high-sensitivity imaging with down to 10 nm surface resolution as well as surface sensitivity in the order of nm when well-controlling the primary ion fluence. The measurement parameters of the Helium Ion Microscope were as follows: the source gas injected into the gas field ion source was Neon, the resulting primary ions Ne^+, the acceleration voltage of the primary ions 25 kV, the column aperture 70 µm and the current was 2.2 pA. The SIMS system parameters were as follows: the sample voltage was -500 V to extract negative secondary ions, the spectrometer acceleration voltage was 3000 V, the analyzed masses were ^{12}C, ^{79}Br and ^{127}I. The images contained 512 x 512 pixels, the raster size was 10 x 10 μm^2 and the counting time 5 ms/pixels.

Micro PL and micro Raman: The measurements were carried out on a Renishaw InVia Raman microscope. PL and Raman mapping was done exclusively on glass-encapsulated devices (encapsulated inside N_2 glovebox using Torr Seal epoxy). The microscope objective is the L100x (spot size of about 400 nm). The PL map was recorded before the Raman map (5% laser intensity) using a 532 nm green laser. No visible degradation signs have been observed after PL mapping. We use a relatively low

excitation density of around 3mW/cm^2 (0.005%) and the light exposure time per measurement of 0.15 seconds. Raman data were fitted using multipeak fitting procedure with Origin 8 program.

Computational Details:

The simulations of the spectroscopic properties of MAFAPbIBr have been carried out with the PWSCF and PHONON packages of Quantum-Espresso[4]. Following the procedure previously reported by some of us[5], the Raman spectrum has been calculated using the LDA approach since Raman intensities are only available in Quantum-Espresso within LDA. LDA has been shown to deliver vibrational frequencies of inorganic perovskites of comparable quality to GGA results[6]. Norm conserving, scalar relativistic pseudo-potentials have been used with electrons from N, C 2s2p, H 1s, Pb 6s6p5d, Br 4s,4p and I 5s5p explicitly included in the calculations. We have chosen a cut-off of 70 Ry for the plane wave expansion and a 2 x 2 x 2 mesh for the sampling of the first Brillouin zone, as a compromise between accuracy and computational cost. Geometry optimization has been carried out by relaxing both the cell parameters and the atomic positions.

AFM/KPFM measurements: The AFM/KPFM measurements were carried out using a Cypher AFM from Asylum Research. Devices were fabricated as specified above (no cathode). The illumination source was white light LED. The devices were exposed to controlled dark/dry air environment until the beginning of the measurements.

Sample storage conditions: An extreme attention has been kept for sample handling and storage in order to have consistent and reproducible data. More in details, the samples for PL/Raman measurements have been prepared and encapsulated in inert atmosphere using a thin glass coverslip to protect the films and enable their storage for weeks. Samples for HIM-SIMS and KPFM were also prepared under inert atmosphere and subsequently stored in permanent dry and dark conditions, together with the solar cells that were fabricated in the same time as control samples.

2. Device characterization

The photovoltaic device performance was analyzed using a VeraSol LED solar simulator (Newport) producing 1 sun AM 1.5 (1000W/m^2) sunlight. Current-voltage curves were measured in air with a potentiostat (Keithley 2604). The light intensity was calibrated with a NREL certified KG5 filtered Si reference diode. The solar cells were masked with a metal aperture of 0.16 cm^2 to define the active area. The current-voltage curves were recorded scanning at 20 mV s^{-1} with 3 sec light soaking before the scan. Hysteresis curves were routinely recorded. Full solar cells were fabricated alongside the half-devices analyzed during this study in order to perform the fundamental characterization on high efficient devices. Figure 1 shows the device characteristics. Batch 1 corresponds to a batch of solar cells fabricated 1 day before batch 2. Note that the samples used for HIM-SIMS and for the optical measurements deliver as control up to 19.8% PCE. Devices for KPFM measurements have been fabricated following the very exact sample preparation conditions with a controlled solar cell delivering nearly 19% PCE.

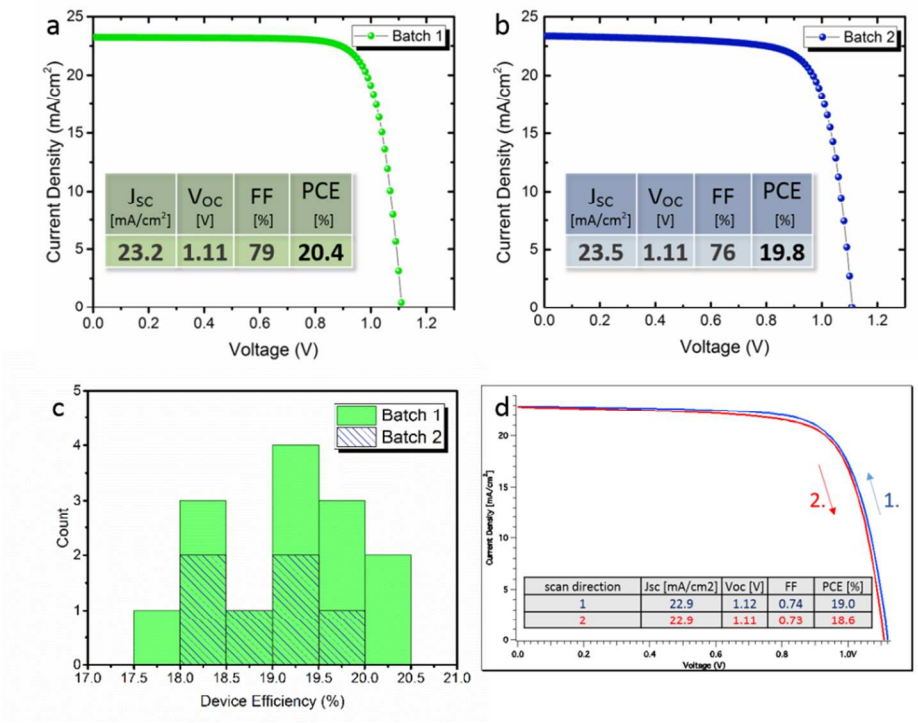

Fig. S1. Device characteristics**. a**. record solar cell with 20.4% PCE for batch 1 and **b.** 19.8% for batch 2. High device reproducibility is shown in **c. d.** Device from b. (initially 19.8%) after storage of 2 months (dark and dry air)

Mixed perovskite: The hole-transporting material polytriarylamine (PTAA) was prepared in toluene (10mg/ml) using the additive Li-bis(trifluoromethanesulfonyl) imide (from a 170 mg/ml Li-TFSI/acetonitrile stock solution) and 4 µl of 4-tert-butylpyridine (TBP). The final HTM solutions were spin-coated on top of the perovskite layers at 3000 rpm for 30 s. The gold electrodes were deposited by thermal evaporation (Kurt Lesker) of 100 nm gold using a shadow mask under high vacuum conditions.

3. Conventional SIMS depth profile

Fig. S2 shows the cross-section SEM image of a mixed perovskite device without cathode (turned 90° anti-clockwise) on top of which the SIMS signals of Pb, Br and I are overlaid. Conventional SIMS with impact energies of the primary ions ranging from a few hundred eV to a few keV provides depth-profile resolution in the range of only a few nanometers, but averaged over the analyzed area, which ranges typically from several hundred μm^2 up to a few mm^2. In the perovskite capping layer, all of the three signals are stable. Once the mesoporous/perovskite interface is reached the signals drop significantly. Roughness of the FTO glass makes the data from this layer less meaningful. However, interestingly, we do not identify significant gradients of Br/I or Pb across the 550 nm depth of the perovskite capping layer.

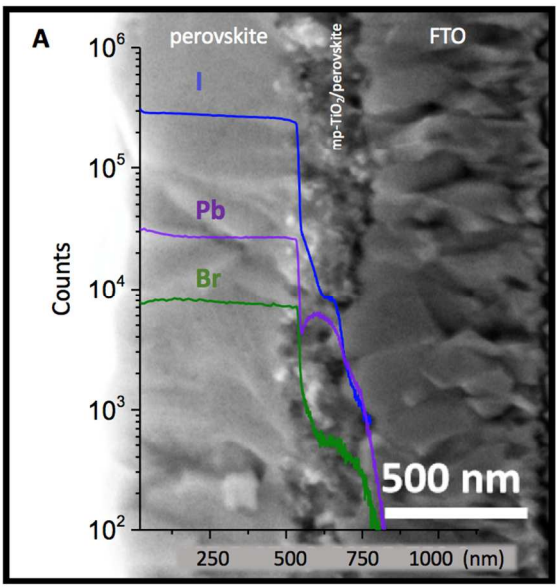

Fig. S2. Conventional Dynamic SIMS depth profile signals overlaid on top of a cross-section SEM image (turned 90° anti-clockwise) of a mixed perovskite solar cell (without cathode). Inside the perovskite capping layer, the Pb, I and Br content shows no significant gradient.

A Conventional Dynamic Secondary Ion Mass Spectrometry instrument (Sc-Ultra, Gennevilliers, France) was used to characterize the mixed perovskite based solar cell in depth profile mode. The experiments reported here were performed using a Cs+ primary ion source with a primary current of 10nA and an impact energy of 3 keV. The positive charged Cs-metal clusters were detected on a whole surface of 60 µm in diameter (area analysed) and the signals were normalized by the Cs+ signal intensity to reduce the matrix effect[7].

4. KPFM characterization

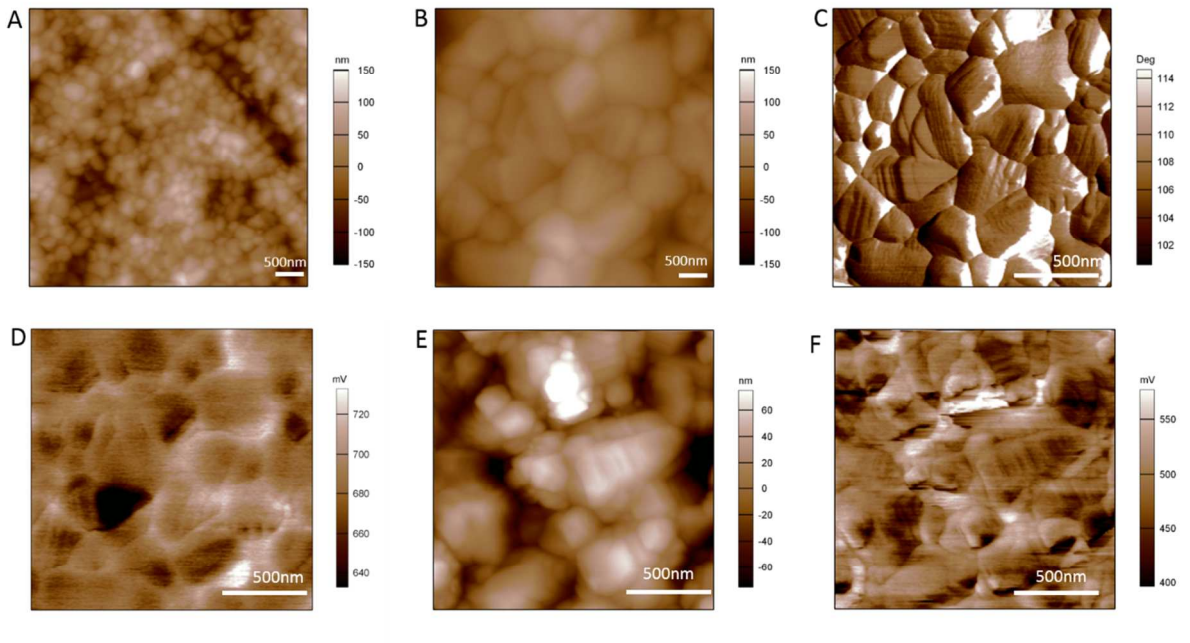

Fig. S3. A: AFM height trace of mixed perovskite (5x5 μm^2), Figure B:AFM height trace of a 1.5x1.5 μm^2 map (mixed perovskite); Figure C: phase of the same 1.5x1.5 μm^2 map (mixed perovskite); Figure D: Surface potential of 1.5x1.5 μm^2 map (mixed perovskite) under white LED illumination; Figure E: height trace (1.5x1.5 μm^2 map) of pure MAPbI3 perovskite; Figure F: Surface potential of pure perovskite in the dark.

5. XRD characterization

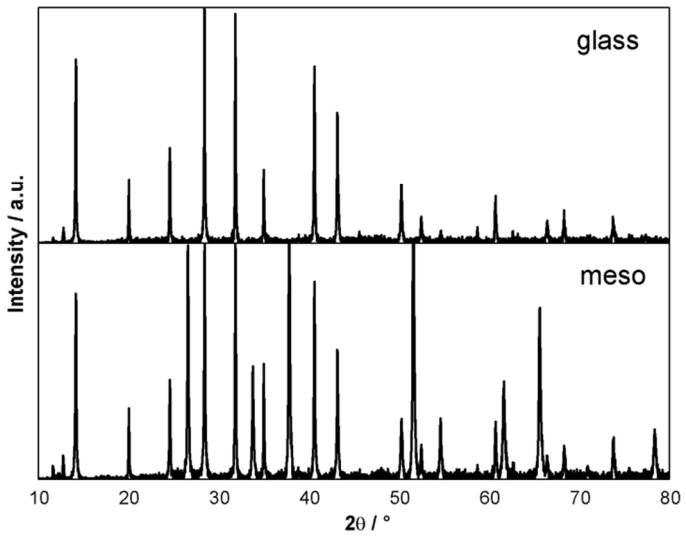

Fig. S4. XRD diffractogram of a mixed perovskite film deposited on glass and infiltrated into a mesoporous TiO_2 scaffold (device architecture).

The X-ray diffractogram of perovskite- (on glass + device) was recorded using a Bruker D8 Advance machine.

6. MicroPL/Raman measurements

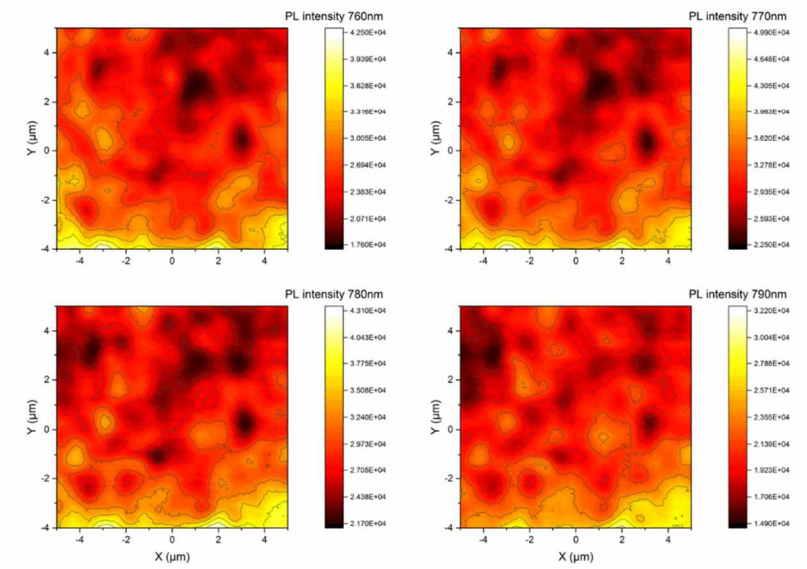

Fig. S5. PL intensity maps of the mixed perovskite capping layer at different emission wavelength (760 nm, 770 nm, 780 nm and 790 nm)

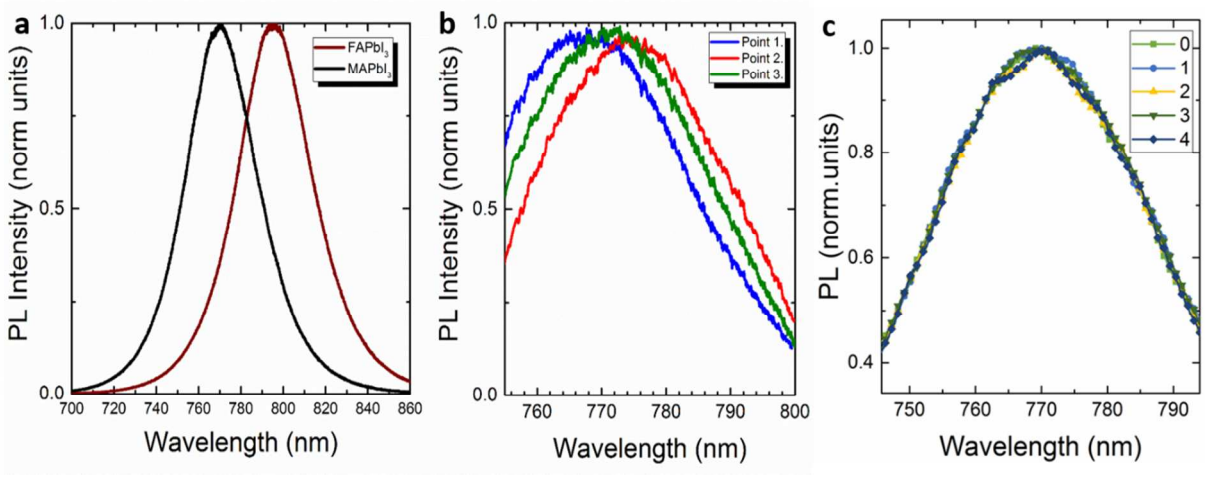

Fig. S6. a. PL spectra of the mixed perovskite capping layer upon excitation at 532nm. **b.** Micro-PL spectra at points 1., 2., 3. as indicated in the main manuscript**. c.** repeated sequential measurements. As reported in the legend 0-4 represent the measurements done sequentially on the same point.

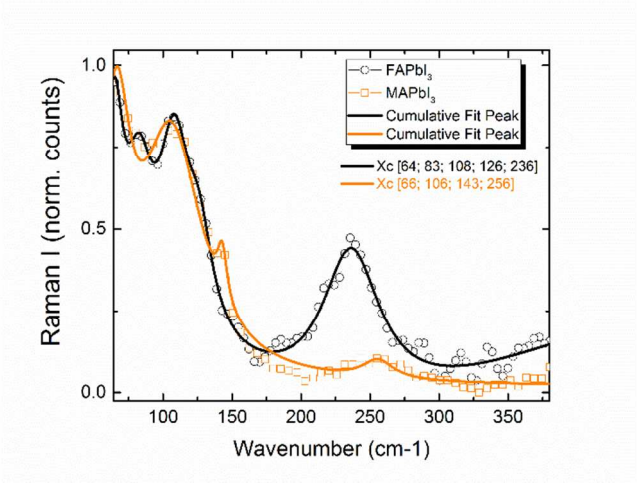

Fig. S7 Raman spectrum of $MAPbI_3$ and $FAPbI_3$. The peak position derived from multi-peaks fitting are listed in the inset as Xc.

7. Theoretical modeling

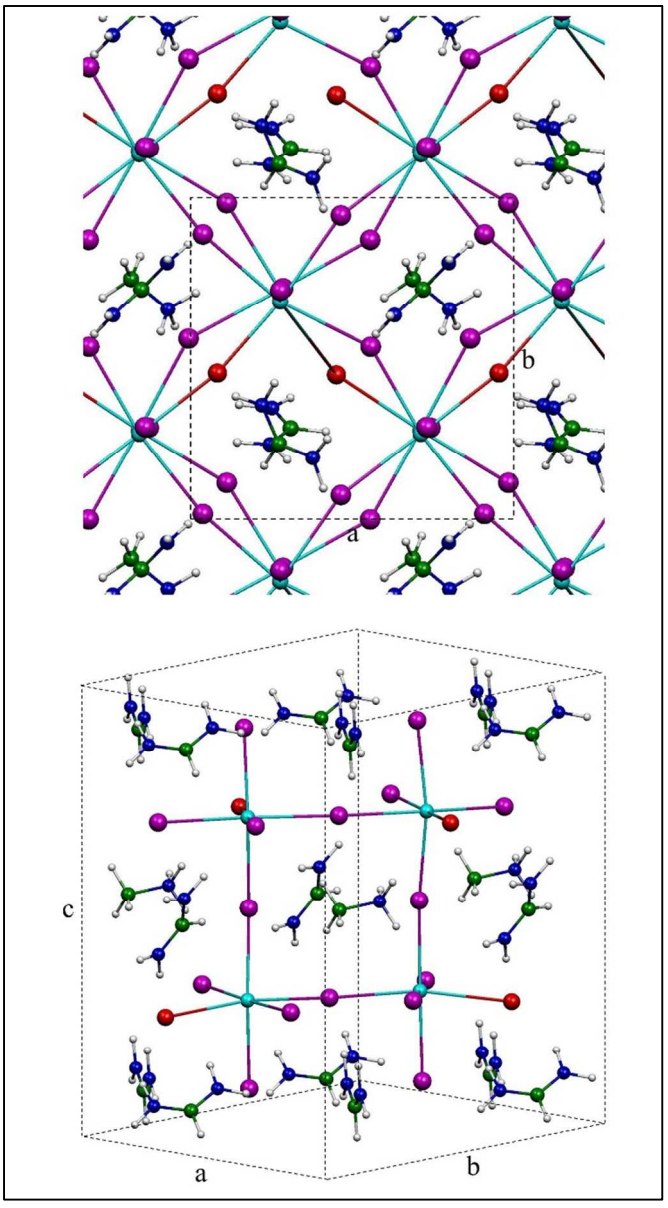

Fig. S8. Optimized geometry of structure 1 (C in green, N in blue, H in grey, I in purple, Pb in cyan and Br in red). The optimized cell parameters are a = b = 8.82 and c = 12.90 Å and the calculated band gap is 1.63 eV.

8. HIM-SIMS details

The lateral resolution reached on commercial SIMS instruments is mostly limited by the brightness of the ion sources used to generate these primary ions[7]. This lateral resolution of 50 nm is well above the ultimate physical limitation of the lateral resolution, which is defined by the lateral dimension of the collision cascade triggered in the sample upon the impact of the primary ions (approximately 8-10nm for typical impact energies in the 10keV range, depending on the sample material and the primary ion species)[8]. In order to further improve the lateral resolution towards the ultimate physical limitation, Wirtz et al. introduced in 2015 SIMS performed with a super high-brightness (~ $4 \cdot 10^9$ A/($cm^2 \cdot sr$)) Gas Field Ion Source (GFIS) delivering He+ and Ne+ ions[9]. The lower sputter yields as well as the lower ionization efficiencies obtained by the light and non-reactive He+ and Ne+ ion beams compared to the heavier and chemically reactive Cs+ and O- beams that are used on conventional SIMS instruments are compensated by the higher bombardment density and Cs and O2 gas flooding during the analysis, respectively[10]. The prototype SIMS spectrometer that was specifically developed by LIST for the HIM-SIMS instrument, that is based on a Zeiss ORION NanoFab platform, allows the detection of all elements/isotopes and small clusters with masses up to 500 amu with a mass resolution M/ΔM greater than 400 and parallel detection of 4 mass channels.

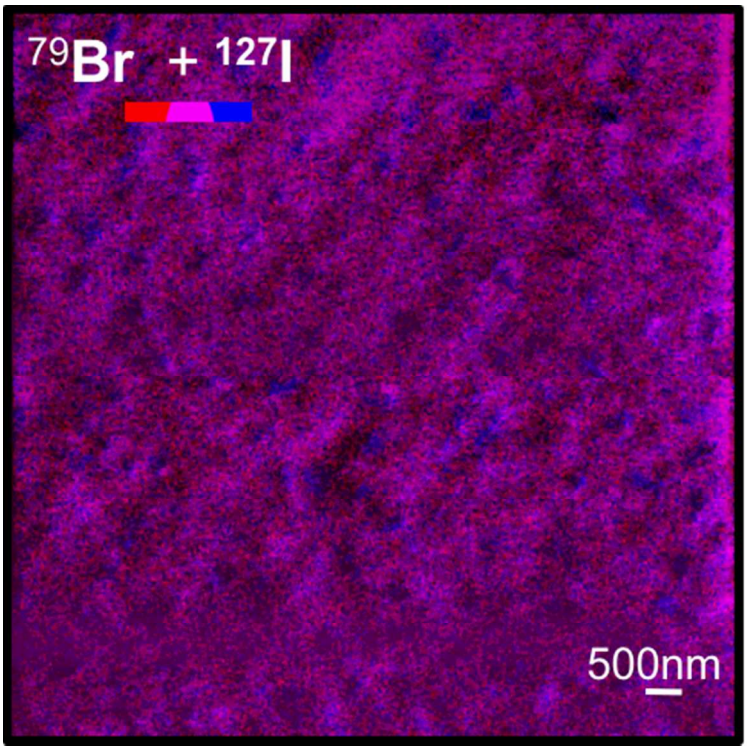

Fig. S9. Elemental nanoscale HIM-SIMS mapping considering the overlap of ^{79}Br (red) and ^{127}I (blue) signals. The "blue" spots have low ^{79}Br signal but high ^{127}I intensities.

References

(1) Giordano, F.; Abate, A.; Correa Baena, J. P.; Saliba, M.; Matsui, T.; Im, S. H.; Zakeeruddin, S. M.; Nazeeruddin, M. K.; Hagfeldt, A.; Graetzel, M. *Nat. Commun.* **2016**, *7*, 10379.

(2) Jeon, N. J.; Noh, J. H.; Kim, Y. C.; Yang, W. S.; Ryu, S.; Seok, S. I. *Nat. Mater.* **2014**, *13*, 897–903.

(3) Eperon, G. E.; Stranks, S. D.; Menelaou, C.; Johnston, M. B.; Herz, L. M.; Snaith, H. J. *Energy Environ. Sci.* **2014**, *7*, 982.

(4) Giannozzi, P.; Baroni, S.; Bonini, N.; Calandra, M.; Car, R.; Cavazzoni, C.; Davide Ceresoli; Chiarotti, G. L.; Cococcioni, M.; Dabo, I.; Corso, A. D.; Gironcoli, S. de; Fabris, S.; Fratesi, G.; Gebauer, R.; Gerstmann, U.; Gougoussis, C.; Anton Kokalj; Lazzeri, M.; Martin-Samos, L.; Marzari, N.; Mauri, F.; Mazzarello, R.; Stefano Paolini; Pasquarello, A.; Paulatto, L.; Sbraccia, C.; Scandolo, S.; Sclauzero, G.; Seitsonen, A. P.; Smogunov, A.; Umari, P.; Wentzcovitch, R. M. *J. Phys. Condens. Matter* **2009**, *21*, 395502.

(5) Quarti, C.; Grancini, G.; Mosconi, E.; Bruno, P.; Ball, J. M.; Lee, M. M.; Snaith, H. J.; Petrozza, A.; Angelis, F. D. *J. Phys. Chem. Lett.* **2014**, *5*, 279–284.

(6) Evarestov, R. A. *Phys. Rev. B* **2011**, *83*, 14105.

(7) Wirtz, T.; Philipp, P.; Audinot, J.-N.; Dowsett, D.; Eswara, S. *Nanotechnology* **2015**, *26*, 434001.